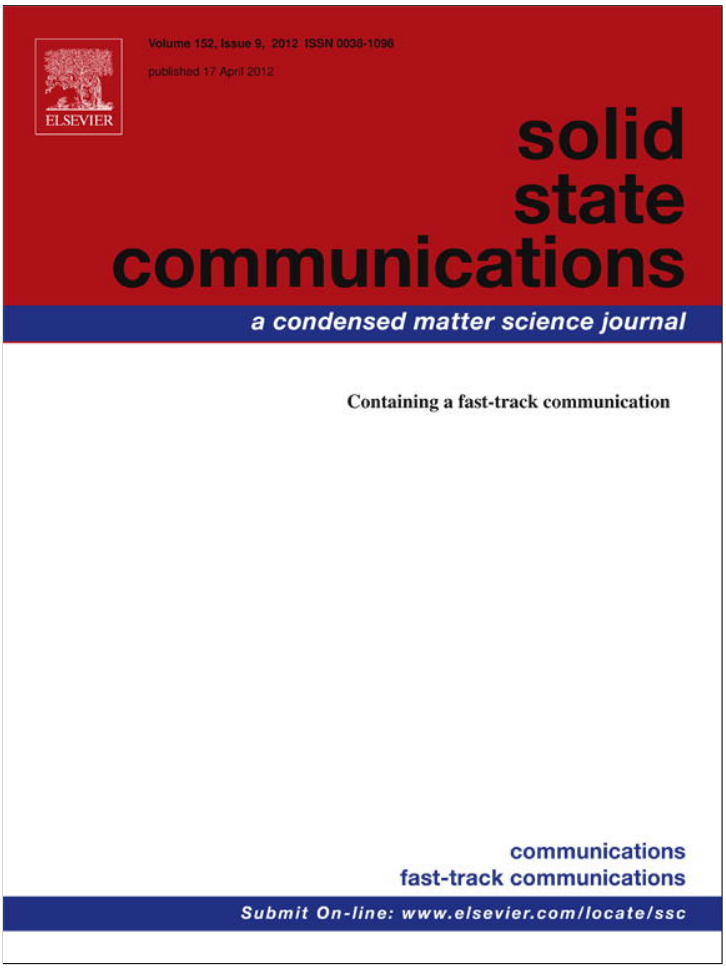

Solid State Communications 152 (2012) 775–778

Contents lists available at SciVerse ScienceDirect

Solid State Communications

journal homepage: www.elsevier.com/locate/ssc

Ab initio calculation of high pressure phases and electronic properties of $CuInSe_2$

Prayoonsak Pluengphon [a], Thiti Bovornratanaraks [a,b,*], Sornthep Vannarat [c], Kajornyod Yoodee [a,b], David Ruffolo [b,d], Udomsilp Pinsook [a,b]

[a] Department of Physics, Faculty of Science, Chulalongkorn University, Bangkok 10330, Thailand
[b] ThEP Center, CHE, 328 Si-Ayuttaya Road, Bangkok 10400, Thailand
[c] Large-Scale Simulation Research Laboratory, National Electronics and Computer Technology Center, Pathumthani 12120, Thailand
[d] Department of Physics, Faculty of Science, Mahidol University, Bangkok 10400, Thailand

ARTICLE INFO

Article history:
Received 30 October 2011
Received in revised form
27 January 2012
Accepted 29 January 2012
by F. Peeters
Available online 3 February 2012

Keywords:
A. Ternary compound
B. sX-LDA
C. High pressure, phase transitions, path of transformation
D. Electrical properties

ABSTRACT

We used an *ab initio* method to calculate the high pressure phases of $CuInSe_2$. By using the experimentally suggested phases, the enthalpy difference showed that the $I\bar{4}2d$ structure transforms into $Fm\bar{3}m$ at 12 GPa and then into *Cmcm* at 42 GPa. The volume reductions at each phase transition are 13.9% and 1.9% respectively, compared with 11% and 1% from experiments. By using the sX-LDA functional, we found that the bandgap in the $I\bar{4}2d$ structure increases at the rate of 39.6 meV/GPa, in fair agreement with photoabsorption experiments. The band gap is closed in the $Fm\bar{3}m$ and *Cmcm* structures. The bond lengths between Cu–Se and In–Se were investigated. We found that the bond lengths can be related to the behavior of the energy gap under high pressure. The path of transformation from $Fm\bar{3}m$ to *Cmcm* was proposed. The energy barrier between the two phases was estimated. The upper bound of the energy barrier is 17 meV which is equivalent to 198 K. This finding can explain the existence of two phases at room temperature reported by experimental study.

1. Introduction

Copper indium diselenide ($CuInSe_2$ or CIS) is a ternary I–III–VI compound. It is a technologically important material which has been widely used in photovoltaic applications and high efficiency solar cells [1–7]. Its high pressure phases were studied by diamond anvil cells and X-ray diffraction experiments [8,9]. Tinoco et al. [8] studied the high pressure phases of CIS up to 29 GPa by using energy dispersive X-rays from synchrotron radiation and a membrane diamond anvil cell. They found that CIS transforms from the chalcopyrite phase ($I\bar{4}2d$) to a NaCl-like cubic phase ($Fm\bar{3}m$) at 7.6 GPa and the volume reduction at the phase transition is about 11%. Recently, Bovornratanaraks et al. [9] extended the study of CIS up to 53.2 GPa. They observed an orthorhombic *Cmcm* structure at 33.9 GPa, and the cubic $Fm\bar{3}m$ phase is completely transformed to *Cmcm* at 43.9 GPa. Apart from the structural phase transitions, the CIS band gap and optical properties under pressure were studied in the chalcopyrite phase [10–12]. Gonźalez and Rinćon [10] studied the optical absorption of monocrystalline CIS samples grown by the Bridgman technique and the chemical vapor transport method. At 300 K, they found that the energy gap increases linearly with pressure between 0 and 7 GPa at the rate of 30 meV/GPa. It was proposed that the band gap increase comes from I–VI bond reduction as a result of *pd* bonding of the valence orbitals under pressure [13]. Recently, by studying $CuInSe_2$, $CuGaSe_2$ and $CuAlSe_2$, Maeda and Wada [14] concluded that *sp* bonding of the III–VI bond dominates the conduction band and a shorter bond length results in a wider band gap. Vidal et al. [15] studied the electronic properties of CIS by using GW and a hybrid functional. They found that the band gap in the chalcopyrite phase depends strongly on the lattice displacement. The trend of the GW band gap was compared with the DFT-LDA results. Despite underestimating the band gap values, the LDA results exhibit a similar trend to the GW results.

However, we found that the *Cmcm* high pressure phases and the electrical properties of CIS in $Fm\bar{3}m$ and *Cmcm* have never been studied by *ab initio* calculation. Therefore, the main aim of the present research was to use an *ab initio* method to study the structural phase transition of CIS under high pressure up to 80 GPa. We reported the transition pressure and volume reduction, compared with experiments. We also gave description on the bonding under pressure for three possible phases. The CIS band structures in all phases were estimated and the trend of gap can be compared and extended with existing experimental and other theoretical data. Furthermore, we proposed the path of

* Corresponding author at: Department of Physics, Faculty of Science, Chulalongkorn University, Bangkok 10330, Thailand.
E-mail address: thiti.b@gmail.com (T. Bovornratanaraks).

0038-1098/$ – see front matter © 2012 Published by Elsevier Ltd
doi:10.1016/j.ssc.2012.01.046

Table 1
The lattice parameters and bulk modulus of CIS at 0 GPa, compared with those of experiments, LDA and FPLAPW theory.

Phase	a (Å)	c/a	B_0 (GPa)	Method
$I\bar{4}2d$	5.7967	2.0071	54.45	GGA this work
	5.7783	2.0026		Expt.[a]
	5.733	1.988	53.22	FPLAPW-LDA[b]
	5.782	2.009		Expt.[c]
			53.6	Expt.[d]
			70.92	LDA[e]

[a] Ref. [9].
[b] Ref. [12].
[c] Ref. [22].
[d] Ref. [23].
[e] Ref. [24].

transformation from the $Fm\bar{3}m$ to the *Cmcm* structure. This allowed us to estimate the potential barrier between the two phases. This can provide a clue on the existence of these two structures, reported by experiments.

2. Calculation details

We used an *ab initio* calculation with the self-consistent field (SCF) method as implemented in the CASTEP code [16,17]. In the SCF loops, all ground state properties are determined by solving Kohn–Sham equations from the density functional theory (DFT) [17]. The generalized-gradient approximation (GGA) functional of Perdew–Burke–Ernzerhof (PBE) [18,19] was adopted for the exchange-correlation energy. In most cases, we have used the ultrasoft pseudopotentials for the atomic cores. The high pressure phases of CIS were taken from experiment [8,9], and are the $I\bar{4}2d$, $Fm\bar{3}m$, and *Cmcm* structures. We calculated the total energy (E) as a function of volume (V). The calculation parameters were optimized by convergent tests, and they are as follows. The energy cutoff was set to 500 eV for the total energy calculations. The electron energy tolerance per atom was 0.01 meV. The Monkhorst–Pack grid size for the SCF calculation was set to $5\times5\times6$ k-points for $I\bar{4}2d$, and $5\times5\times5$ for the $Fm\bar{3}m$ and *Cmcm* phases. The E–V data points were fitted to the 3rd order Birch–Murnaghan equation of state (EOS) [20,21]. The stability of the high pressure phases was determined from the lowest enthalpy, $H = E + PV$. We calculated the CIS energy gap and the electronic band structure at each pressure by using sX-LDA with $3\times3\times4$ k-points, an energy cutoff of 800 eV and a norm-conserving pseudopotential. We also used a higher energy cutoff at 880 eV, and it gave a slightly different total energy within the range of 5 meV.

3. Results and discussion

In order to verify our calculation, we calculated the $I\bar{4}2d$ structure at 0 GPa and compared it with the existing theoretical and experimental data, as shown in Table 1. The results showed good agreement in terms of the lattice parameters and the bulk modulus. This gave us confidence to proceed further.

Next, we calculated the E–V data points of the three different phases and fitted them to the EOSs, as shown in Fig. 1. The E–V curves showed that the $I\bar{4}2d$ phase has lowest energy at equilibrium volume, and the lowest energy shifted to the $Fm\bar{3}m$ and *Cmcm* structures respectively as the volume decreased. Then we calculated the enthalpy (H) as a function of the pressure (P). The inset of Fig. 1 is the enthalpy difference, using the $I\bar{4}2d$ enthalpy as a reference. The H–P curve clearly showed that CIS with the $I\bar{4}2d$ structure transforms into the $Fm\bar{3}m$ structure at 12 GPa, and then to the *Cmcm* structure at 42 GPa.

In addition, we plotted the volume–pressure relation, as shown in Fig. 2. This relation provided the information on the volume

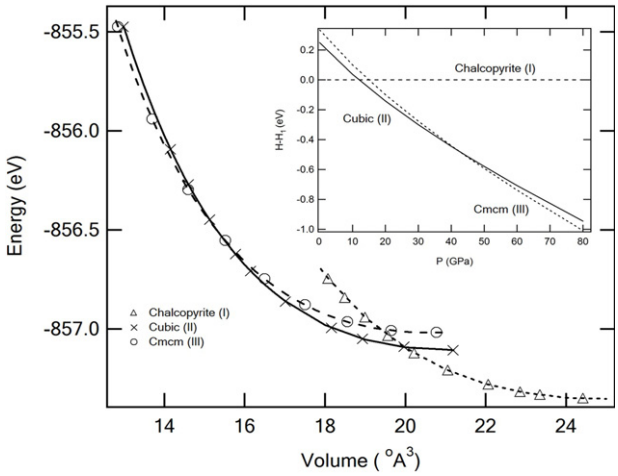

Fig. 1. E–V data points of the three phases and their fitted EOSs. The inset shows the enthalpy difference as a function of pressure. The enthalpy of the $I\bar{4}2d$ phase was used as a reference.

Table 2
Summary of the transition pressure and the volume reduction at each phase transition, compared with the experimental data in parentheses from Bovornratanaraks et al. [9].

Transition pressure (GPa)	$-\Delta V$ (%)	Phase transition
12 (7)	13.9 (11)	$I\bar{4}2d$ to $Fm\bar{3}m$
42 (39)	1.9 (1)	$Fm\bar{3}m$ to *Cmcm*

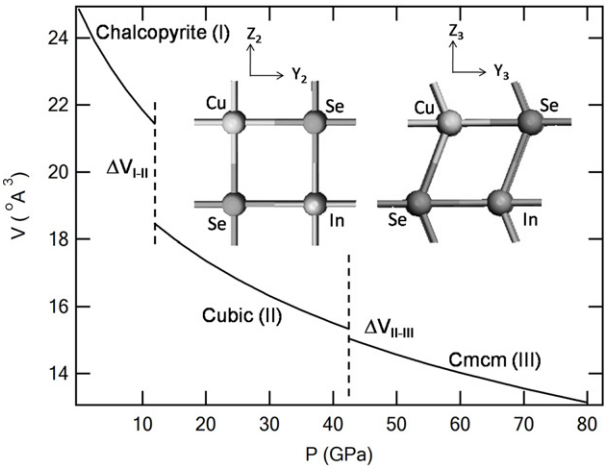

Fig. 2. The equations of state (V–P relation) of the three phases of CIS between 0 and 80 GPa. This V–P curve allowed us to find the volume reduction at each phase transition. The inset shows the atomic movements as CIS transforms from the $Fm\bar{3}m$ to the *Cmcm* structure.

reduction at each phase transitions. We found that the volume reduction at the $I\bar{4}2d$ to $Fm\bar{3}m$ transition is 13.9%, and that at the $Fm\bar{3}m$ to *Cmcm* transition is 1.9%, compared with 11% and 1% respectively from the experiments [8,9]. The transition pressures and the volume reductions are summarized and compared with existing data from the experiment [9] in Table 2. It is readily seen that the calculation gave a good description of the experiment [9].

From the *ab initio* calculation, we obtained also the optimized atomic positions of each phases. The $Fm\bar{3}m$ and *Cmcm* atomic positions in the y–z plane are shown in the inset of Fig. 2. The atomic visualization in the inset allowed us to construct the model of the transformation path from the $Fm\bar{3}m$ to the *Cmcm* structure. First, the Cu–Se layers in the xy plane move relatively parallel to the In–Se layers. The magnitude of the relative atomic movement is 20% in the y axis. Second, the phase transition also involves some

Table 3
The CIS band gap from sX-LDA and the trend of the gap under pressure, compared with FPLAPW [12], LDA [24], sX-LDA [14] and experimental results [10,11].

Structure	Band gap (eV)	$\Delta E_g/\Delta P$ (meV/GPa)	Method
$I\bar{4}2d$ (0 GPa)	0.680	39.6	sX-LDA[a]
	0.913 (5 GPa)	39.6	sX-LDA[a]
	1.076 (10 GPa)	39.6	sX-LDA[a]
	0.98	30	Expt.[b]
	1.04	29	Expt.[c]
	0.26	–	FPLAPW-LDA[d]
	0.96	–	sX-LDA[e]
	0.12	31	LDA[f]
$Fm\bar{3}m$ (15 GPa)	Vanished	–	sX-LDA[a]
Cmcm (50 GPa)	Vanished	–	sX-LDA[a]

[a] This work.
[b] Ref. [10].
[c] Ref. [11].
[d] Ref. [12].
[e] Ref. [14].
[f] Ref. [24].

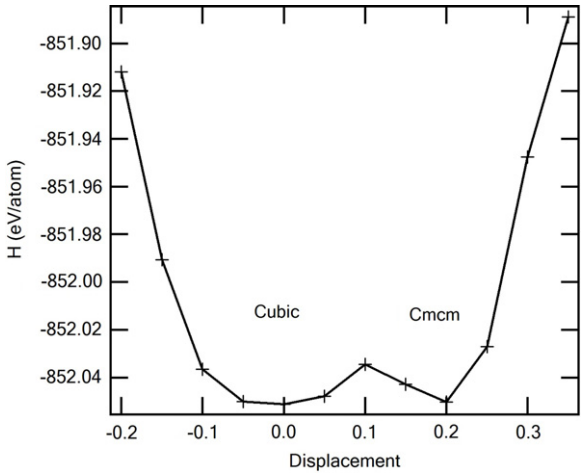

Fig. 3. The enthalpy along the path of transformation. It showed the two distinguish energy wells of the NaCl-like cubic and the *Cmcm* phases, and also the barrier of 17 meV, equivalent to 198 K.

small strain because the shape of the unit cell changes and the volume reduces during the phase transition. By taking all these changes into the account, we calculated the enthalpy along the path by starting at the perfect $Fm\bar{3}m$ phase and moving the Cu–Se layer along the *y* axis at each step by 0.05 in the reduced cell units. After a few movement steps, the phase transition is completed and the *Cmcm* structure is obtained. The result of the enthalpy along the transformation path is shown in Fig. 3. Hence, our simulated path of transformation has provided the upper bound to the barrier between the two phases. It is an upper bound because the exact path of transformation will always have lowest enthalpy. From Fig. 3, we found that the barrier height is 17 meV per atom or equivalent to the thermal energy at 198 K. This finding can be used to explain the co-existence of the $Fm\bar{3}m$ and *Cmcm* phases. In fact, this co-existence was reported in the X-ray diffraction experiment [9], where the *Cmcm* structure firstly appeared at 33.9 GPa in the $Fm\bar{3}m$ phase, then they co-existed in the pressure range of 33.9–43.9 GPa. The complete phase transition to the *Cmcm* structure occurred at 43.9 GPa onward.

Next, we calculated the band gaps of the three phases. It is widely known that the local scheme of DFT gives good description for the ground state of the system only. However, the energy gap calculation involves the excitation states and the local exchange-correlation functional can be inaccurate. For example, the GGA typically underestimates the band gap. Thus, we resorted to the sX-LDA functional. It uses a non-local screened exchange scheme combined with an LDA correlation functional, and should provide a better energy functional than the purely local scheme of the LDA or GGA [14]. Indeed, our gap values were in fair agreement with experimental data and other theoretical studies. We found that the sX-LDA band gap at 0 GPa is 0.680 eV in the chalcopyrite ($I\bar{4}2d$) phase, and the band gap increases as pressure increases. The increase rate of the band gap is 39.6 meV/GPa, compared with 30 meV/GPa from optical absorption experiments [10,11,24]. In the $Fm\bar{3}m$ and *Cmcm* phases, the band gap vanishes because of the overlap between the valence band maximum (VBM) and the conduction band minimum (CBM), as shown in Fig. 4. The electronic density of states (EDOS) suggested also the semiconductor to metallic transition. Typical band structures of the $I\bar{4}2d$ and $Fm\bar{3}m$ structures are shown in Fig. 4(a) and (b). The results of the sX-LDA gap values are summarized in Table 3. It is well known that the LDA or GGA band gaps are underestimated. Zhang et al. [25] showed that the band gap of CIS at 0 GPa is 0.17 eV from the LDA but it can be corrected by adding a constant shift of 1.04 eV from experiments. However the LDA band gaps exhibit a similar trend compared with experiments. Moreover, Vidal et al. [15] showed that the LDA band gap can be corrected by a scissor operator and gives better values compared with the GW band gap.

Table 4
The bond lengths of the closest Cu–Se and In–Se pairs under pressure.

Bond length (Å)	*P* (GPa)					
	0	5	10	15	40	60
Cu–Se	2.42	2.36	2.31	2.64	2.48	2.50
In–Se	2.65	2.59	2.55	2.64	2.47	2.45

In addition, we have investigated the bond length and its relation to the band gap. Maeda and Wada [14] explained that the valence band of CIS is dominated by Cu 3*d* and Se 4*p* whereas the conduction band is dominated by In 5*s* and Se 4*p*. They also showed that in an isolated $CuSe_4$ or $InSe_4$ molecule, the energy levels split due to covalent bonding. The key feature is that the proximity of atoms in the molecule strengthens the bonding, and the energy levels split further apart. Then, they replaced the In atom by a Ga or Al atom and found that the III–VI bonds are shortened. These shortened bonds are accompanied by a widening band gap in the bulk I–III–VI compounds, as expected. This situation is similar to CIS under high pressure where all the bonds are shortened, see Table 4, and the band gap is widened in the $I\bar{4}2d$ phase (0–12 GPa). Thus, this is just the effect of the stronger bonding under high pressure. However, at the $I\bar{4}2d$ to $Fm\bar{3}m$ phase transition, the Cu–Se and In–Se bonds become longer. This is surprising at first because we would expect a more packed structure under high pressure. By looking closely at the $I\bar{4}2d$ structure, we found that a Cu atom is coordinated by 4 Se atoms, the same as an In atom which is also coordinated by 4 Se atoms. After the phase transition to the $Fm\bar{3}m$ structure, the Cu atom is coordinated by 6 Se atoms, so as the In atom. Thus, the total structure is still more packed under pressure, even though the bond lengths are longer.

4. Conclusions

In this research, we have used an *ab initio* method to calculate the high pressure phases of CIS. We found that CIS transforms from the $I\bar{4}2d$ structure to the $Fm\bar{3}m$ structure at 12 GPa and then into the *Cmcm* structure at 42 GPa. The volume reductions at the phase transitions are 13.9% and 1.9% respectively. The sX-LDA band gap in the $I\bar{4}2d$ structure increases at the rate of 39.6 meV/GPa, in fair agreement with 30 meV/GPa from the photoabsorption experiment [10,11,24]. We found that the band gap is closed in the $Fm\bar{3}m$ and *Cmcm* structures. We investigated the nature of bonding in CIS under pressure, and gave an explanation of the

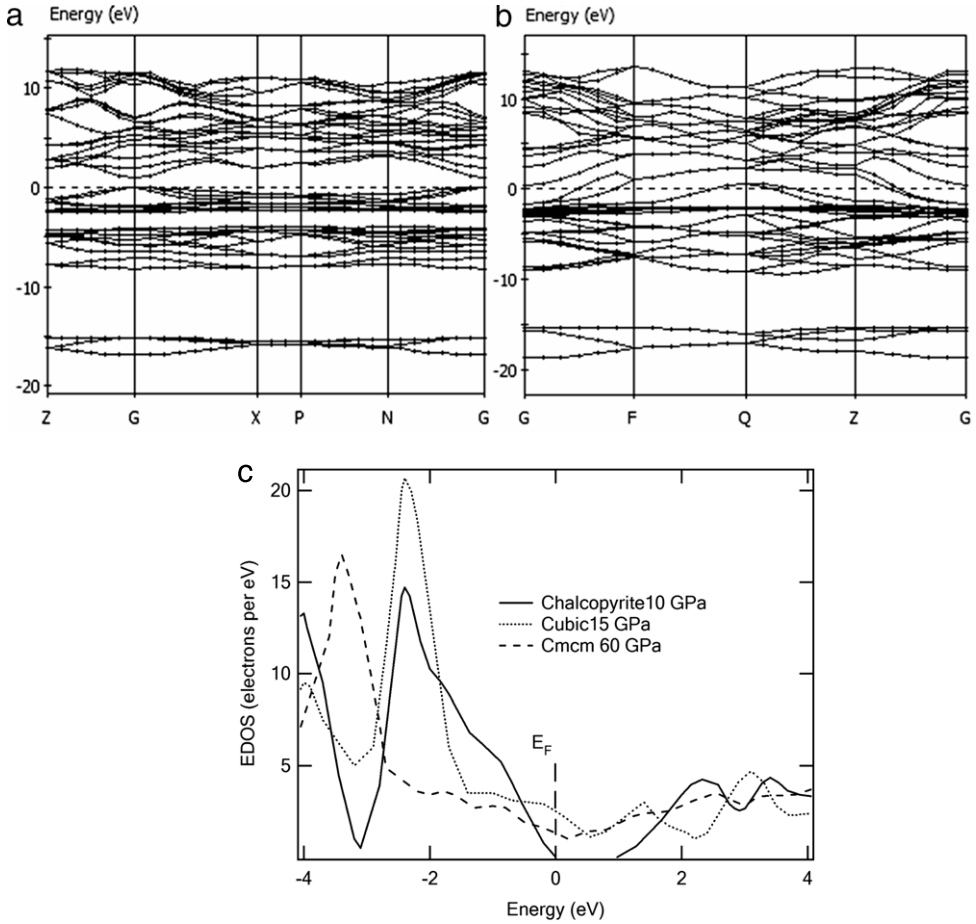

Fig. 4. Comparison of the energy bands of CIS from sX-LDA. (a) The energy band of the chalcopyrite phase at 5 GPa with a gap of 0.913 eV. (b) The energy band of the NaCl-like phase at 15 GPa. Notice that the VBM and CBM are overlapping. The Fermi level was set as a reference at 0 eV. (c) The electronic density of states (EDOS) of the high pressure phases of CIS. The gap closure is obvious in the cubic and *Cmcm* phases.

gap closure during the $I\bar{4}2d$ to $Fm\bar{3}m$ phase transition. The path of transformation from $Fm\bar{3}m$ to *Cmcm* was proposed. The barrier between the two phases was estimated. The upper bound of the potential barrier is 17 meV which is equivalent to 198 K. We can explain the existence of two phases at room temperature reported by experimental study [9].

Acknowledgments

P. Pluengphon is supported by Thailand Graduate Institute of Science and Technology (TGIST), 90th Year Chulalongkorn Scholarship from Graduate School Chulalongkorn University. T. Bovornratanaraks acknowledges financial support from Asahi Glass Foundation, National Research Council of Thailand and Thailand Research Fund contract number DBG5280002. The computing facilities are supported by The National Research University Project of CHE and the Ratchadaphiseksomphot Endowment Fund (FW657B).

References

[1] A. Rockett, R.W. Birkmire, J. Appl. Phys. 70 (1991) R82.
[2] A. Zegadi, M.A. Slifkin, M. Djamin, R.D. Tomlinson, H. Neumann, Solid State Commun. 83 (1992) 587.
[3] J. Krustok, J. Mädasson, K. Hjelt, H. Collan, Solid State Commun. 94 (1995) 889.
[4] C. Rincón, Solid State Commun. 64 (1987) 15.
[5] H. Neumann, B. Perlt, N.A.K. Abdul-Hussein, R.D. Tomlinson, A.E. Hill, Solid State Commun. 42 (1982) 855.
[6] H. Neumann, R.D. Tomlinson, Solid State Commun. 57 (1986) 591.
[7] S. Kohiki, M. Nishitani, T. Negami, T. Wada, Phys. Rev. B 45 (1992) 9163.
[8] T. Tinoco, A. Polian, D. Gomez, J.P. Itie, Phys. Status Solidi (b) 198 (1996) 433.
[9] T. Bovornratanaraks, V. Saengsuwan, K. Yoodee, M.I. McMahon, C. Hejny, D. Ruffolo, J. Phys.: Cond. Matt. 22 (2010) 355801.
[10] J. Gonźalez, C. Rinćon, J. Appl. Phys. 65 (1991) 2031.
[11] I. Choi, P.Y. Yu, Phys. Status Solidi (b) 211 (1996) 143.
[12] M. Belhadj, A. Tadjer, B. Abbar, Z. Bousahafs, H. Aourag, Phys. Stat. Sol. (b) 241 (2004) 2516.
[13] J.E. Jaffe, A. Zunger, Phys. Rev. 29 (1984) 1982.
[14] T. Maeda, T. Wada, Japan J. Appl. Phys. 49 (2010) 04DP07.
[15] J. Vidal, S. Botti, P. Olsson, J. Guillemoles, L. Reining, Phys. Rev. Lett. 104 (2010) 056401.
[16] M.C. Payne, M.P. Teter, D.C. Allan, T.A. Arias, D. Joannopoulos, Rev. Modern Phys. 64 (1992) 1045.
[17] M.D. Segall, P.L.D. Lindan, M.J. Probert, C.J. Pickard, P.J. Hasnip, S.J. Clark, M.C. Payne, J. Phys.: Cond. Matt. 14 (2002) 2717.
[18] J.P. Perdew, J.A. Chevary, S.H. Vosko, K.A. Jackson, M.R. Pederson, D.J. Singh, C. Fiolhais, Phys. Rev. B 46 (1992) 6671.
[19] J.P. Perdew, K. Burke, M. Ernzerhof, Phys. Rev. Lett. 77 (1996) 3865.
[20] F. Birch, Phys. Rev. 71 (1947) 809.
[21] F.D. Murnaghan, Proc. Natl. Acad. Sci. USA 30 (1944) 244.
[22] J. Parkets, R.D. Tomlinson, J. Hampshire, J. Appl. Cryst. 6 (1973) 414.
[23] H. Neuman, Phys. Status Solidi (b) 96 (1986) K121.
[24] S. Wei, A. Zunger, I.H. Choi, P.Y. Yu, Phys. Rev. B 58 (1998) R1710.
[25] S.B. Zhang, S. Wei, A. Zunger, H. Katayama-Yoshida, Phys. Rev. B 57 (1998) 9642.